

Volcanic, coseismic, and seasonal changes detected at white Island (Whakaari) volcano, New Zealand, using seismic ambient noise

A.S. Yates, M.K. Savage, A.D. Jolly, Corentin Caudron, I.J. Hamling

▶ **To cite this version:**

A.S. Yates, M.K. Savage, A.D. Jolly, Corentin Caudron, I.J. Hamling. Volcanic, coseismic, and seasonal changes detected at white Island (Whakaari) volcano, New Zealand, using seismic ambient noise. Geophysical Research Letters, 2019, 46 (1), p. 99-108. 10.1029/2018GL080580 . hal-02295450

HAL Id: hal-02295450
https://hal.science/hal-02295450

Submitted on 1 Sep 2021

HAL is a multi-disciplinary open access archive for the deposit and dissemination of scientific research documents, whether they are published or not. The documents may come from teaching and research institutions in France or abroad, or from public or private research centers.

L'archive ouverte pluridisciplinaire **HAL**, est destinée au dépôt et à la diffusion de documents scientifiques de niveau recherche, publiés ou non, émanant des établissements d'enseignement et de recherche français ou étrangers, des laboratoires publics ou privés.

Copyright

Check for updates

AGU100 ADVANCING EARTH AND SPACE SCIENCE

Geophysical Research Letters

RESEARCH LETTER
10.1029/2018GL080580

Key Points:
- Individual three-component seismic stations are well suited to monitoring at locations with sparse seismic coverage
- Volcanic, coseismic, and seasonally induced velocity changes highlight the complexity when interpreting ambient noise results
- Distant seismic stations provide a useful comparison to distinguish between volcanic and nonvolcanic processes

Supporting Information:
- Supporting Information S1

Correspondence to:
A. Yates,
alec.yates@vuw.ac.nz

Citation:
Yates, A. S., Savage, M. K., Jolly, A. D., Caudron, C., & Hamling, I. J. (2019). Volcanic, coseismic, and seasonal changes detected at White Island (Whakaari) volcano, New Zealand, using seismic ambient noise. *Geophysical Research Letters*, *46*, 99–108. https://doi.org/10.1029/2018GL080580

Received 21 SEP 2018
Accepted 10 DEC 2018
Accepted article online 19 DEC 2018
Published online 3 JAN 2019

©2018. American Geophysical Union. All Rights Reserved.

Volcanic, Coseismic, and Seasonal Changes Detected at White Island (Whakaari) Volcano, New Zealand, Using Seismic Ambient Noise

A. S. Yates[1], M. K. Savage[1], A. D. Jolly[2], C. Caudron[3,4], and I. J. Hamling[2]

[1]School of Geography, Environment and Earth Sciences, Victoria University of Wellington, Wellington, New Zealand, [2]GNS Science, Avalon, New Zealand, [3]Department of GeologyGhent University, Campus Sterre, Ghent, Belgium, [4]ISTerre, Université de Savoie, IRD, CNRS, Le Bourget du Lac, France

Abstract Ambient noise interferometry is becoming increasingly popular for studying seismic velocity changes. Such changes contain information on the structural and mechanical properties of Earth systems. Application to monitoring, however, is complicated by the large number of processes capable of inducing crustal velocity changes. We demonstrate this at White Island volcano over a 10-year period containing multiple well-documented eruptions. Using individual seismic stations, we detect velocity perturbations that we ascribe to volcanic activity, large earthquakes, and seasonality. Distant seismic stations capture widespread nonvolcanic changes that are also present at the volcano. Comparison between velocity changes recorded by distant and local stations then allows us to distinguish volcanic phenomena from seasonality. Through this, we resolve distinct features in ambient noise-derived velocity changes that relate to volcanic unrest and a phreatic eruption, illustrating the strength of the approach.

Plain Language Summary Detecting small changes in physical properties at volcanoes is important toward effectively forecasting volcanic eruptions. One approach is to monitor the speed of seismic waves at the Earth's surface, which are sensitive to changes in the rock they pass through. At volcanoes, such changes may manifest through subsurface pressure increases preceding eruptions. Correctly interpreting these changes, however, is complicated. Many other, nonvolcanic, processes are also capable of producing similar wave speed perturbations. At White Island volcano, New Zealand, we detect changes associated with volcanic activity, large earthquakes, and weather-related processes using seismometers located on the volcano. We demonstrate that volcanic and nonvolcanic features can be distinguished by comparing changes recorded at the volcano with those recorded at large distances, where volcanic changes are not expected to be observed. Through this, we resolve distinct differences that can be related to volcanic activity, illustrating the strength of this approach.

1. Introduction

Volcano monitoring aims to detect subtle changes at volcanoes where magma ascent, or the disturbance of a shallow magma reservoir, is expected to induce crustal deformation (Patanè et al., 2003; Sparks, 2003). Recent advances in seismology have allowed seismic velocity changes to be measured at volcanoes through ambient noise interferometry (e.g., Anggono et al., 2012; Brenguier, Shapiro, et al., 2008; Brenguier et al., 2011; Duputel et al., 2009; Mordret et al., 2010; Sens-Schönfelder & Wegler, 2006). This traditionally uses the cross-correlation of seismic noise recorded by two stations to reveal surface waves traveling between them (Sabra et al., 2005; Shapiro & Campillo, 2004; Shapiro et al., 2005). Seismic velocity changes are then retrieved by analyzing temporal variations in the resultant cross-correlation functions. Such changes contain information on structural and mechanical changes within hydrothermal and magmatic systems.

Volcanoes are capable of producing varied seismic velocity patterns. Recent studies have identified both velocity increases and decreases preceding eruptions, sometimes occurring in different locations simultaneously (Anggono et al., 2012; Budi-Santoso & Lesage, 2016; Donaldson et al., 2017; Obermann et al., 2013). This could reflect distinct deformational styles dependant on the relative position of the pressure source (Budi-Santoso & Lesage, 2016; Donaldson et al., 2017).

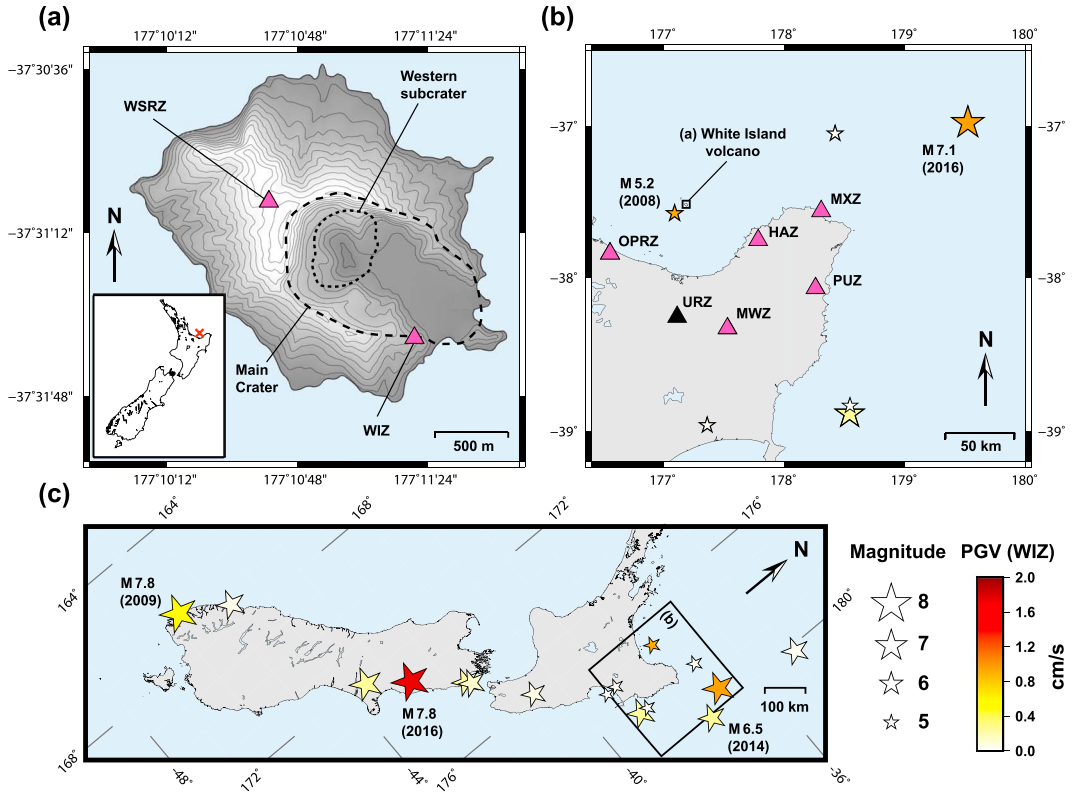


Figure 1. Map of the study region with significant nearby tectonic earthquakes shown (stars), colored according to the PGV measured at White Island (Table S3). Earthquakes recording the five largest values are labeled (magnitude and year). Permanent seismic stations used are displayed as pink triangles, and nearby unused stations as black triangles. (a) Map of White Island volcano (25-m contours), with its location within New Zealand shown in inset (red cross). Main Crater and the western subcrater are drawn following Moon et al. (2005). (b) Map of onshore seismic stations. (c) Earthquakes investigated between 2007 and 2017 (Table S3). PGV = Peak Ground Velocity.

Many other natural phenomena have also been found to produce measurable velocity changes using ambient noise. These include coseismic and postseismic changes following tectonic earthquakes (e.g., Brenguier, Campillo, et al., 2008; Chen et al., 2010; Heckels et al., 2018; Lesage et al., 2014; Minato et al., 2012), rainfall (e.g., Hillers et al., 2014; Rivet et al., 2015; Sens-Schönfelder & Wegler, 2006), atmospheric pressure loading (e.g., Niu et al., 2008; Silver et al., 2007), atmospheric-temperature-induced thermoelasticity (e.g., Hillers et al., 2015; Richter et al., 2014), tidal modulation (e.g., Takano et al., 2014; Yamamura et al., 2003), and artificial changes related to variation in the noise source (e.g., Hillers & Ben-Zion, 2011; Snieder, 2006). Critically, the amplitudes of velocity changes resulting from these influences can be similar to those resulting from volcanic phenomena. Thus, it remains difficult to distinguish between the various processes inducing crustal velocity changes.

We apply ambient noise interferometry at White Island (Whakaari in Māori), an active stratovolcano located approximately 50 km offshore (Figure 1). Eruptions are predominantly phreatic, phreatomagmatic, and strombolian in style, typically emitting only small volumes of eruptive material (Cole et al., 2000; Houghton & Nairn, 1991). The upper kilometer hosts a large volcano-hydrothermal system, beneath Main Crater (Figure 1a), with all recent activity and outgassing confined to the western subcrater (Giggenbach & Glasby, 1977; Nishi et al., 1996). Magma driving the eruptions are thought to originate from magma reservoirs as shallow as 500 m, with evidence of deeper reservoirs located between 1–2 and 2–7 km depth (Cole et al., 2000; Houghton & Nairn, 1989).

Recent activity began in 2012 (supporting information Table S1) following over a decade of relative inactivity. White Island experienced five ash and steam eruptions, numerous small mud eruptions and geysering, and extruded a small lava dome during a highly active period between August 2012 and October 2013 (Chardot

et al., 2015; Jolly et al., 2016). Activity resumed in 2016 with a moderate phreatic eruption in April followed by a minor ash emission in September, thought to have resulted from vent erosion (GeoNet, 2016a).

2. Data and Methods

White Island has sparse seismic coverage, with only two permanent three-component seismometers located on the volcano (Figure 1a). Only one of these (WIZ) has been active throughout recent activity (Table S2), handicapping station-pair correlation approaches. One alternative is to cross-correlate the different components of individual seismic stations, with recent work (Bennington et al., 2018; De Plaen et al., 2016) showing encouraging similarities when compared to velocity changes measured using the traditional two station approach. We therefore apply this technique at White Island, with its sparse seismic coverage providing an excellent test case for single-station monitoring.

Seismic data are acquired from seven three-component broadband stations that make up part of the permanent GeoNet network between 2007 and 2017. Two of these stations—WIZ and WSRZ—are located on the volcano (Figure 1a), while the other five stations—HAZ, MWZ, MXZ, OPRZ, and PUZ—are located onshore (Figure 1b). These are used to gain an understanding of background velocity changes in the region. Station URZ is excluded as only vertical-component data were acquired.

We also process real-time seismic amplitude measurements (RSAM) and access interferometric synthetic aperture radar (InSAR) data previously processed for White Island (Hamling, 2017). RSAM data are computed by band passing raw, vertical-component, seismic data—recorded at WIZ—and computing the RMS amplitude in 1-min intervals. The mean for each day is then calculated to give a daily sampling interval. We apply band pass filters between 1.2 and 5.0 Hz, corresponding to the bandwidth of volcanic tremor at White Island (Chardot et al., 2015; Jolly et al., 2016; Sherburn et al., 1998), and 0.1 and 1.0 Hz to match the frequency band used to estimate velocity changes.

Seismic data are processed through to velocity changes using the Python package MSNoise (Lecocq et al., 2014), using the same parameters for all stations. The data are first band pass filtered between 0.1 and 1.0 Hz, resampled to 10 Hz, and temporally normalized through clipping data at three times the RMS. If processing single-station cross-components, where different components of a single station are cross-correlated with each other, spectral whitening is applied. If cross-correlating each component with itself, producing auto-correlations, no whitening is applied as information is only contained within the amplitude spectrum. This makes auto-correlations sensitive to changes in the source of seismic noise in addition to changes in the medium (Hobiger et al., 2014). Finally, the data are cross-correlated in 2-hr time slices and the resultant cross-correlation functions stacked linearly to 10 days to improve temporal stability. This set of parameter choices was found to maximize the SNR of cross-correlation functions (Figure S1), after assessment of 1-bit normalization, different length time slices, and phase-weighted stacking (see also Yates, 2018).

Temporal velocity changes are computed using the moving-window cross-spectral analysis method (Clarke et al., 2011; Poupinet et al., 1984). Delay times are measured between individual 10-day stacks and a reference stack—computed using all available 1-day stacks—in a series of 16-s moving windows. The final velocity change is calculated from the slope of the delay times ($\delta t/t$):

$$\frac{\delta t}{t} = -\frac{\delta v}{v}, \tag{1}$$

where $\delta v/v$ is the relative velocity variation (Lecocq et al., 2014; Ratdomopurbo & Poupinet, 1995). Only delay times within lags of 20 and 80 s are used—from both sides of the cross-correlation function—with additional quality control requirements on the maximum delay time (0.4 s), maximum error (0.1 s), and minimum coherence (0.7) between the individual and reference stack (Lecocq et al., 2014). Alternative parameter choices are demonstrated in Figures S2 and S3. We finish with six independent time series for each station. These are split into the auto-correlations (EE, NN, ZZ components) and the cross-components (EN, EZ, NZ) after performing a weighted arithmetic mean based on the error in $\delta t/t$.

We also compute Pearson's correlation coefficient between individual and reference stacks within minimum and maximum lag times. The correlation coefficient here is the average calculated from both the positive and negative sides of the cross-correlation function. Decorrelation between waveforms can indicate changes in the scattering of seismic energy (Haney et al., 2015; Obermann et al., 2013). At volcanoes, this may reflect structural changes associated with volcanic activity (e.g., Obermann et al., 2013). Such changes may be temporary,

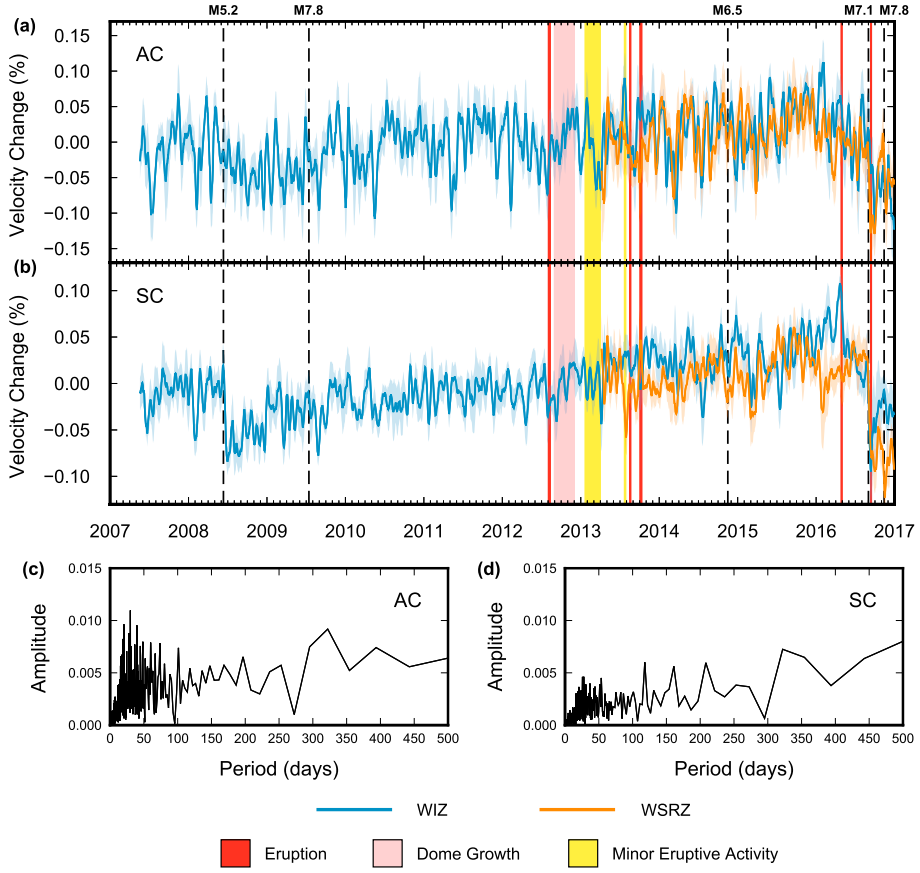


Figure 2. Velocity changes for AC and SC at WIZ (blue line) and WSRZ (orange line). Velocity changes are smoothed using a 14-day centered moving-window mean for visual clarity, with ±1 standard error shaded around the mean line. Eruptive activity is split into categories of eruptions, dome growth, and minor eruptive activity (following Table S1), color-coded following the key. The times of significant tectonic earthquakes—labeled in Figure 1—are also shown (vertical dashed lines). (a) AC velocity changes. (b) SC velocity changes. (c) Fast Fourier Transform of unsmoothed AC velocity changes. (d) Fast Fourier Transform of unsmoothed SC velocity changes. AC = auto-correlations; SC = cross-components.

for example, through the opening and closing of microcracks (e.g., Nur & Simmons, 1969a; Ratdomopurbo & Poupinet, 1995), or permanent through irreversible structural damage.

3. Results

3.1. Velocity Changes at White Island

White Island stations show strong short-term fluctuations throughout the study period (Figure 2). These are larger for auto-correlations (Figure 2a), with measurements made using the cross-components found to be more stable through time (Figure 2b). This is consistent with previous studies, where the reduced stability of auto-correlations is thought to result from the inability to apply spectral whitening (e.g., De Plaen et al., 2016; Hobiger et al., 2014). Spectral properties of velocity changes at WIZ do not reveal a clear systematic pattern to short-term changes (Figures 2c and 2d), as might be expected if influenced by the 14-day tidal stress cycle. We do not explore the source of these changes further, simply acknowledging that such fluctuations reduce the ability to interpret velocity changes on time scales less than a few weeks.

Coseismic velocity decreases are distinctly evident at White Island, especially in the cross-component analysis (Figure 2b). The first decrease occurs at the time of a M_W 5.2 earthquake in 2008 (Figure 2), located approximately 10 km from the volcano (Figure 1b). We also identify a velocity decrease at the time of the M_W 7.1 Te Araroa earthquake in 2016 (Figures 2 and S4), located over 200 km away from the volcano (Figure 1b). This is detected in both auto-correlations and cross-component correlations at WIZ and WSRZ (Figures 2a and 2b). Both earthquakes recorded large peak ground velocities at White Island relative to others investi-

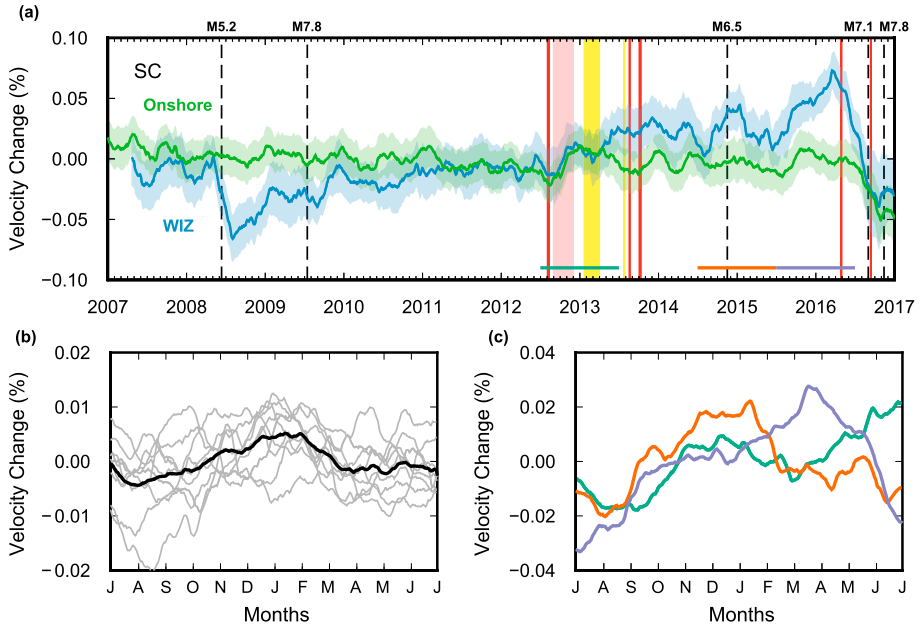


Figure 3. Onshore SC velocity changes are compared with changes at White Island. (a) Velocity changes at WIZ (blue) and onshore (green) after being smoothed using a 90-day centered moving-window mean to emphasize seasonal characteristics. Note that this artificially gives the impression of precursory earthquake decreases rather than coseismic changes (e.g., Figures S4 and S5). Tectonic and eruptive activity is shown following the key in Figure 2. (b) Yearly, demeaned, onshore velocity changes are overlain between July and July of each subsequent year (gray lines), with the mean trend shown (black line). (c) Individual years at WIZ are shown following the key in (a), where colored lines above the axis denote the time period. SC = cross-components.

gated (~1 cm/s), with only the M_W 7.8 Kaikōura earthquake producing a larger value (Figure 1c and Table S3). Velocity decreases associated with the Kaikōura earthquake, however, are not as readily distinguishable from background fluctuations (Figures 2a, 2b, and S4).

Long-term velocity changes at WIZ show an increasing trend that begins following the coseismic decrease in 2008, reaching a maximum at the time of the April 2016 eruption (Figure 2). Again, this is best revealed by the cross-components (Figure 2b), with the long-term increase partially concealed in the auto-correlations by strong fluctuations (Figure 2a). At WSRZ, a similar increase is not observed before the April 2016 eruption, with velocity changes recorded at both stations becoming separated from early-2016 (Figure 2b). Following the April 2016 eruption, velocities at WIZ decline rapidly to pre-2015 levels within 2–3 months, while changes at WSRZ remain relatively steady (Figure 2b). Both sites then experience large coseismic velocity decreases associated with the Te Araroa earthquake.

3.2. Comparison With Onshore Stations

Velocity changes recorded at White Island are compared to measurements made onshore by averaging the results from HAZ, MWZ, MXZ, and PUZ (Figure 3). OPRZ is excluded from this analysis due to anomalous measurements that strongly influence the onshore trend (Figure S6). We also exclude auto-correlations from this comparison, with onshore velocity changes poorly recovered (Figure S7). Focusing on the cross-components, we observe strong similarities in the timing of velocity peaks, suggestive of an environmental process (Figures 3a and 3b). We also observe a velocity decrease onshore at the time of the M_W 7.1 earthquake (Figures 3a and S5), indicating a widespread regional change, and find evidence for a further decrease following the M_W 7.8 Kaikōura earthquake (Figure S5). Missing, however, is the velocity decrease in 2008 associated with the M_W 5.2 earthquake, including the subsequent 2- to 3-year recovery period. This is not surprising given the earthquake's close proximity to the volcano (Figure 1b).

Overlaying individual years of onshore velocity changes reveals clear seasonality, with peak velocities during New Zealand summer months (Figure 3b). The source of observed seasonality in noise measurements, however, remains uncertain when compared with meteorological data sets (Yates, 2018). Absent a more complete understanding, we use the agreement between peaks at White Island and onshore to distinguish between vol-

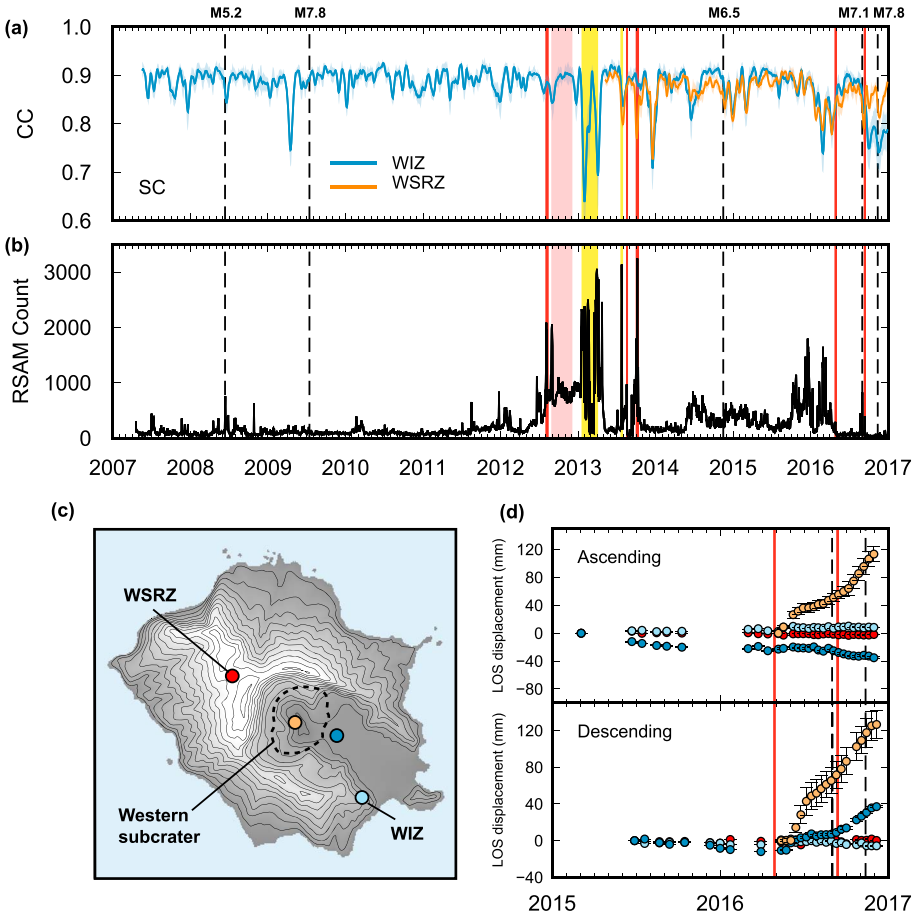


Figure 4. Correlation coefficients, RSAM levels, and interferometric synthetic aperture radar time series are displayed in relation to eruptive and seismic activity, following the key in Figure 2. (a) CCs calculated for WIZ and WSRZ after being smoothed using a 14-day moving-window mean. (b) RSAM data filtered between 1.2 and 5.0 Hz. (c) Map of White Island with points acquired from interferometric synthetic aperture radar shown. (d) LOS displacements are shown for points displayed in (c), matched by color. Increases in LOS displacement indicate motion away from the satellite, implying subsidence. Both ascending (top) and descending (bottom) tracks are shown. RSAM = real-time seismic amplitude measurements; CC = correlation coefficient; SC = cross-components; LOS = line-of-sight.

canic and meteorological processes. In 2012–2013, velocities at White Island resemble the seasonal cycle until early-2013, with further increases then deviating from the onshore trend (Figure 3c). Similarly, in early-2016, the velocity recorded at White Island peaks a couple months later than might be expected for the seasonal cycle (Figure 3c). The magnitude of this increase is also larger than any annual peaks observed both onshore and at the volcano. Thus, velocity increases in early-2013 and preceding the April 2016 eruption are not likely to be related to a seasonal influence.

4. Discussion

4.1. Driving Mechanism

Two periods of velocity increase are detected in cross-component velocity changes at WIZ that cannot be explained by seasonality or by postseismic recovery (Figure 3). The first occurs during a volcanically active period in 2012–2013 and the second in the months preceding the April 2016 eruption (Figure 3c). Both coincide with increased RSAM activity (Figure 4b), suggestive of increased tremor activity, and decreases in the correlation coefficient (Figure 4a). For changes in the correlation coefficient, the lack of a clear change in 0.1–1.0 Hz RSAM (Figure S8) suggests these decreases are not related to data contamination through increased volcano seismicity. Also, the correlation coefficient does not appear to suffer during increased RSAM levels in 2012 (Figure 4). We therefore interpret that decorrelation during minor activity in 2013 and in the months preceding the April 2016 eruption are suggestive of short-term structural changes at the volcano.

Note, however, that changes in the correlation coefficient at WIZ from September 2016 are likely related to a sensor change (Table S2).

Interpretations of seismic velocity changes at volcanoes commonly call upon variations in the distribution of microcracks (e.g., Ratdomopurbo & Poupinet, 1995). Laboratory experiments have shown that when pressures increase, seismic velocities increase through the closing of cracks (Nur, 1971). At larger pressures, the development of new cracks results in a seismic velocity decrease as the surrounding rock deforms (Lockner et al., 1977; Nur & Simmons, 1969b). Velocity increases recorded here could therefore be interpreted to reflect cracks closing under increased pressures beneath the volcano. However, identifying the physical source of velocity changes at volcanoes remains a complex problem (e.g., Azzola et al., 2018; Snieder, 2006), requiring further research.

InSAR data acquisition beginning in early-2015 provides insight into the surface deformation accompanying velocity changes. In the year preceding the April 2016 eruption, line-of-sight decreases in both ascending and descending tracks around the crater floor (dark blue in Figures 4c and 4d) are consistent with uplift (Figure S9). At points coincident with WIZ and WSRZ, however, line-of-sight changes are minimal. This suggests a shallow source, with the modeled ~100 m source depth (Hamling, 2017) consistent with depth estimates for similar uplift episodes at the volcano (Fournier & Chardot, 2012). Such episodes are thought to be related to increased pore pressures within the hydrothermal system (Fournier & Chardot, 2012). It is not surprising then that the velocity changes recorded by WIZ and WSRZ do not parallel each other (Figure 2b), as might be expected for a deeper pressure source. Further, the observation of a velocity increase associated with a shallow inflation source supports strain modeling by Donaldson et al. (2017).

Following the April 2016 eruption, line-of-sight increases are recorded within the western subcrater, indicative of posteruptive subsidence (Figures 4d and S9). This contrasts with deformation observed around the lake edge, where varied behavior in ascending and descending tracks represents posteruptive slumping of the crater wall (Hamling, 2017). The timing of crater floor subsidence coincides with a rapid decline in the seismic velocity at WIZ, a recovery of the correlation coefficient at both stations, and reduced RSAM levels that resemble pre-2011 behavior (Figures 2b and 4). We interpret this to reflect a reduction in pressure beneath the volcano following the April 2016 eruption, resulting in deflation at the surface and reduced seismic velocities.

Interestingly, the observed subsidence is much larger in magnitude than the uplift recorded prior to the April 2016 eruption (Figure 4d). This could be indicative of accumulated uplift prior to the acquisition of InSAR data. If the velocity increase in early-2013 reflects an increase in pressure, then the lack of a subsequent velocity decrease following eruptive activity in October 2013 would suggest pressures have remained elevated. Such an interpretation is consistent with increased RSAM levels continuing through 2014 and 2015 (Figure 4b). The increased magnitude of subsidence following the April 2016 eruption, relative to earlier uplift, may then reflect the elimation of a long-term pressure source, with the volcano returning to a relatively inactive state. While ash venting in September 2016 may indicate otherwise, the timing of this renewed activity is curious given the M_W 7.1 Te Araroa earthquake 2 weeks earlier. It is possible then that the earthquake influenced the timing of this event. As of mid-2018, no further eruptive activity has been recorded at the volcano.

4.2. Volcanic Versus Nonvolcanic Sources

Volcano monitoring using ambient noise is complicated by the large number of processes capable of producing measurable velocity changes. Recent studies have tried to apply corrections for changes induced by rainfall (e.g., Budi-Santoso & Lesage, 2016; Lecocq et al., 2017; Rivet et al., 2015; Wang et al., 2017) and thermoelastic strain (e.g., Lecocq et al., 2017). However, discriminating between the different environmental processes remains a complex problem, with seasonal changes likely to be a product of multiple sources. Furthermore, the crustal response to external processes can vary significantly between different regions (Wang et al., 2017), increasing the analysis required to perform reliable corrections.

At White Island, we use distant seismic stations to distinguish between volcanic and nonvolcanic processes. This has the advantage of providing a simple comparison data set, while not requiring assumptions about the source of externally induced changes. We identify clear deviations from background behavior during eruptive activity in 2013 and in the months preceding the April 2016 eruption (Figure 3). Further, the detection of a coseismic velocity decrease onshore following the M_W 7.1 Te Araroa earthquake confirms its widespread impact, allowing similar decreases at White Island to be classified as nonvolcanic despite preceding volcanic

activity. Thus, distant seismic stations may allow local volcanic processes to be distinguished from more widespread nonvolcanic processes.

An interesting finding of this study is the striking velocity changes caused by nearby tectonic earthquakes (Figures 2, S4, and S5). Earthquake-induced velocity changes are well established, with numerous examples of coseismic and postseismic deformation detected using ambient noise (e.g., Brenguier, Campillo, et al., 2008; Chen et al., 2010; Heckels et al., 2018; Lesage et al., 2014; Minato et al., 2012). At volcanoes, these changes have been related to mechanical weakening of the crust following the passage of seismic waves (Brenguier et al., 2014; Lesage et al., 2014). Following the approach of Brenguier et al. (2014), we calculate the seismic velocity susceptibility at White Island (Table S3), defined as the ratio between observed velocity decreases and estimated dynamic stress changes. This has been proposed as a proxy for determining fluid pressurization in volcanic systems (Brenguier et al., 2014). Both the M_W 5.2 and the M_W 7.1 Te Araroa earthquake record a susceptibility of approximately 1.0×10^{-2} MPa^{-1} (Table S3), an order of magnitude larger than those calculated by Brenguier et al. (2014) following the Tohoku-Oki earthquake. Interestingly, despite having recorded the largest ground motions (Table S3), coseismic velocity decreases associated with the M_W 7.8 Kaikōura earthquake are ambiguous. For a susceptibility of 1.0×10^{-2} MPa^{-1}, the expected velocity drop would be over 0.15%. The absence of such a coseismic change may be related to the close temporal proximity of the Te Araroa earthquake, with seismic velocities yet to recover by the time of the Kaikōura event two months later.

5. Conclusions

We apply a single-station approach to ambient noise monitoring at White Island volcano. Seismic velocity increases are identified during volcanic activity in 2012–2013 and in the months preceding a phreatic eruption in April 2016. InSAR measurements show surface uplift accompanied the velocity increase in 2016, while posteruptive subsidence accompanied a velocity decrease following the eruption. The agreement of these data sets highlights the capability of individual seismic stations to detect volcanic changes in an environment unsuitable for the traditional approach to ambient noise interferometry.

Nonvolcanic sources of velocity change are also detected at White Island, highlighting the complexity involved when interpreting ambient noise results. Coseismic velocity decreases are distinctly evident after large earthquakes, followed by periods of postseismic recovery. We also identify environmentally induced changes, with strong similarities between velocities recorded at the volcano and those recorded over a wider region. Comparison between distant and local seismic stations then allowed us to distinguish changes related to volcanic phenomena. However, the observation of many controlling processes highlights the need for an improved understanding of background behavior in order to correctly interpret short-term velocity changes.

Acknowledgments
This project was possible through publicly available seismic data provided by GeoNet (www.geonet.org.nz). The White Island Digital Elevation Model was acquired through the LINZ Data Service (www.linz.govt.nz). A.Y. was supported by the Rachael Westergaard Memorial scholarship—funded by the Westergaard family—and a Victoria University scholarship. M.S. was partly funded by the New Zealand Ministry of Business, Innovation and Employment (MBIE) ECLIPSE Grant (contract CONT-52100-ENDRP-RSCHTRUSTVIC). A.J. and I.H. were partly funded by the Strategic Science Investment Fund (SSIF) from the New Zealand MBIE. Finally, we thank Editor Rebecca Carey, reviewer Gerrit Olivier, and an anonymous reviewer for their comments leading to an improved manuscript.

References

Anggono, T., Nishimura, T., Sato, H., Ueda, H., & Ukawa, M. (2012). Spatio-temporal changes in seismic velocity associated with the 2000 activity of Miyakejima volcano as inferred from cross-correlation analyses of ambient noise. *Journal of Volcanology and Geothermal Research*, *247-248*, 93–107. https://doi.org/10.1016/j.jvolgeores.2012.08.001

Azzola, J., Schmittbuhl, J., Zigone, D., Magnenet, V., & Masson, F. (2018). Direct modeling of the mechanical strain influence on coda wave interferometry. *Journal of Geophysical Research: Solid Earth*, *123*, 1–18. https://doi.org/10.1002/2017JB015162

Bennington, N., Haney, M., Thurber, C., & Zeng, X. (2018). Inferring magma dynamics at Veniaminof volcano via application of ambient noise. *Geophysical Research Letters*, *45*, 11,650–11,658. https://doi.org/10.1029/2018GL079909

Brenguier, F., Campillo, M., Hadziioannou, C., Shapiro, N. M., Nadeau, R. M., & Larose, E. (2008). Postseismic relaxation along the San Andreas Fault at Parkfield from continuous seismological observations. *Science*, *321*(September), 1478–1481.

Brenguier, F., Campillo, M., Takeda, T., Aoki, Y., Shapiro, N. M., Briand, X., et al. (2014). Mapping pressurized volcanic fluids from induced crustal seismic velocity drops. *Science*, *345*(6192), 80–82.

Brenguier, F., Clarke, D., Aoki, Y., Shapiro, N. M., Campillo, M., & Ferrazzini, V. (2011). Monitoring volcanoes using seismic noise correlations. *Comptes Rendus - Geoscience*, *343*(8-9), 633–638.

Brenguier, F., Shapiro, N. M., Campillo, M., Ferrazzini, V., Duputel, Z., Coutant, O., & Nercessian, A. (2008). Towards forecasting volcanic eruptions using seismic noise. *Nature Geoscience*, *1*(2), 126–130.

Budi-Santoso, A., & Lesage, P. (2016). Velocity variations associated with the large 2010 eruption of Merapi volcano, Java, retrieved from seismic multiplets and ambient noise cross-correlation. *Geophysical Journal International*, *206*(1), 221–240.

Caudron, C., Taisne, B., Neuberg, J., Jolly, A. D., Christenson, B., Lecocq, T., et al. (2018). Anatomy of phreatic eruptions. *Earth, Planets and Space*, *70*(1), 168. https://doi.org/10.1186/s40623-018-0938-x

Chardot, L., Jolly, A. D., Kennedy, B. M., Fournier, N., & Sherburn, S. (2015). Using volcanic tremor for eruption forecasting at White Island volcano (Whakaari), New Zealand. *Journal of Volcanology and Geothermal Research*, *302*, 11–23. https://doi.org/10.1016/j.jvolgeores.2015.06.001

Chen, J. H., Froment, B., Liu, Q. Y., & Campillo, M. (2010). Distribution of seismic wave speed changes associated with the 12 May 2008 Mw 7.9 Wenchuan earthquake. *Geophysical Research Letters*, *37*, L18302. https://doi.org/10.1029/2010GL044582

Clarke, D., Zaccarelli, L., Shapiro, N. M., & Brenguier, F. (2011). Assessment of resolution and accuracy of the Moving Window Cross Spectral technique for monitoring crustal temporal variations using ambient seismic noise. *Geophysical Journal International*, *186*(2), 867–882.

Cole, J. W., Thordarson, T., & Burt, R. M. (2000). Magma origin and evolution of White Island (Whakaari) volcano, Bay of plenty, New Zealand. *Journal of Petrology*, *41*(6), 867–895.

De Plaen, R. S. M., Lecocq, T., Caudron, C., Ferrazzini, V., & Francis, O. (2016). Single station monitoring of volcanoes using seismic ambient noise. *Geophysical Research Letters*, *43*, 8511–8518. https://doi.org/10.1002/2016GL070078

Donaldson, C., Caudron, C., Green, R. G., Thelen, W. A., & White, R. S. (2017). Relative seismic velocity variations correlate with deformation at Ki-lauea volcano. *Science Advances*, *3*, 1–12.

Duputel, Z., Ferrazzini, V., Brenguier, F., Shapiro, N., Campillo, M., & Nercessian, A. (2009). Real time monitoring of relative velocity changes using ambient seismic noise at the Piton de la Fournaise volcano (La Reunion) from January 2006 to June 2007. *Journal of Volcanology and Geothermal Research*, *184*(1-2), 164–173. https://doi.org/10.1016/j.jvolgeores.2008.11.024

Fournier, N., & Chardot, L. (2012). Understanding volcano hydrothermal unrest from geodetic observations: Insights from numerical modeling and application to White Island volcano, New Zealand. *Journal of Geophysical Research*, *117*, B11208. https://doi.org/10.1029/2012JB009469

GeoNet (2016a). End of Minor Eruptive Activity at White Island (Whakaari). Volcanic Alert Bulletin. Retrieved from https://www.geonet.org.nz/vabs/2OKryhG5ElyaMkoyy0ScOC

GeoNet (2016b). Volcanic unrest continues at White Island (Whakaari); details of April 27 eruption unravelling. Volcanic Alert Bulletin.

Giggenbach, W. F., & Glasby, G. P. (1977). The influence of thermal activity on the trace metal distribution in marine sediments around White Island, New Zealand. *New Zealand Department of Science and Industrial Research Bulletin*, *218*, 121–126.

Gomberg, J., & Agnew, D. (1996). The accuracy of seismic estimates of dynamic strains: An evaluation using strainmeter and seismometer data from Pinon Flat Observatory, California. *Bulletin of the Seismological Society of America*, *86*(1 SUPPL. A), 212–220.

Hamling, I. J. (2017). Crater lake controls on volcano stability: Insights from White Island, New Zealand. *Geophysical Research Letters*, *44*, 11,311–11,319. https://doi.org/10.1002/2017GL075572

Haney, M. M., Hotovec-Ellis, A. J., Bennington, N. L., De Angelis, S., & Thurber, C. H. (2015). Tracking changes in volcanic systems with seismic interferometry. *Encyclopedia of Earthquake Engineering*, 3767–3786.

Heckels, R. E. G., Savage, M. K., & Townend, J. (2018). Postseismic velocity changes following the 2010 Mw 7 . 1 Darfield earthquake , New Zealand , revealed by ambient seismic field analysis. *Geophysical Journal International*, *213*(2), 931–939.

Hillers, G., & Ben-Zion, Y. (2011). Seasonal variations of observed noise amplitudes at 2-18 Hz in southern California. *Geophysical Journal International*, *184*(2), 860–868.

Hillers, G., Ben-Zion, Y., Campillo, M., & Zigone, D. (2015). Seasonal variations of seismic velocities in the San Jacinto fault area observed with ambient seismic noise. *Geophysical Journal International*, *202*(2), 920–932. https://doi.org/10.1093/gji/ggv151

Hillers, G., Campillo, M., & Ma, K. F. (2014). Seismic velocity variations at TCDP are controlled by MJO driven precipitation pattern and high fluid discharge properties. *Earth and Planetary Science Letters*, *391*, 121–127.

Hobiger, M., Wegler, U., Shiomi, K., & Nakahara, H. (2014). Single-station cross-correlation analysis of ambient seismic noise: Application to stations in the surroundings of the 2008 Iwate-Miyagi Nairiku earthquake. *Geophysical Journal International*, *198*(1), 90–109.

Houghton, B. F., & Nairn, I. A. (1989). The phreatomagmatic and Strombolian eruption events at White Island volcano 1976-82: Eruptive narrative. *NZ Geol Surv Bull*, *103*, 13–23.

Houghton, B. F., & Nairn, I. A. (1991). The 1976-1982 Strombolian and phreatomagmatic eruptions of White Island, New Zealand: Eruptive and depositional mechanisms at a 'wet' volcano. *Bulletin of Volcanology*, *54*(1), 25–49.

Jolly, A., Kennedy, B., Edwards, M., Jousset, P., & Scheu, B. (2016). Infrasound tremor from bubble burst eruptions in the viscous shallow crater lake of White Island, New Zealand, and its implications for interpreting volcanic source processes. *Journal of Volcanology and Geothermal Research*, *327*, 585–603. https://doi.org/10.1016/j.jvolgeores.2016.08.010

Jolly, A., Lokmer, I., Christenson, B., & Thun, J. (2018). Relating gas ascent to eruption triggering for the April 27, 2016, White Island (Whakaari), New Zealand eruption sequence. *Earth, Planets and Space*, *70*(1), 177. https://doi.org/10.1186/s40623-01%8-0948-8

Jolly, A. D., Lokmer, I., Thun, J., Salichon, J., Fry, B., & Chardot, L. (2017). Insights into fluid transport mechanisms at White Island from analysis of coupled very long-period (VLP), long-period (LP) and high-frequency (HF) earthquakes. *Journal of Volcanology and Geothermal Research*, *343*, 75–94. https://doi.org/10.1016/j.jvolgeores.2017.06.006

Larose, E., Roux, P., & Campillo, M. (2007). Reconstruction of Rayleigh-Lamb dispersion spectrum based on noise obtained from an air-jet forcing. *The Journal of the Acoustical Society of America*, *122*(6), 3437–3444. https://doi.org/10.1121/1.2799913

Lecocq, T., Caudron, C., & Brenguier, F. (2014). MSNoise, a python package for monitoring seismic velocity changes using ambient seismic noise. *Seismological Research Letters*, *85*(3), 715–726. https://doi.org/10.1785/0220130073

Lecocq, T., Longuevergne, L., Pedersen, H. A., Brenguier, F., & Stammler, K. (2017). Monitoring ground water storage at mesoscale using seismic noise: 30 years of continuous observation and thermo-elastic and hydrological modeling. *Scientific Reports*, *7*(1), 14241. https://doi.org/10.1038/s41598-017-14468-9

Lesage, P., Reyes-Dávila, G., & Arámbula-Mendoza, R. (2014). Large tectonic earthquakes induce sharp temporary decreases in seismic velocity in Volcán de Colima, Mexico. *Journal of Geophysical Research: Solid Earth*, *119*, 4360–4376. https://doi.org/10.1002/2013JB010884

Lockner, D., Walsh, J., & Byerlee, J. (1977). Changes in seismic velocity and attenuation during deformation of granite. *Journal of Geophysical Research*, *82*(33), 5374–5378.

Minato, S., Tsuji, T., Ohmi, S., & Matsuoka, T. (2012). Monitoring seismic velocity change caused by the 2011 Tohoku-oki earthquake using ambient noise records. *Geophysical Research Letters*, *39*, L09309. https://doi.org/10.1029/2012GL051405

Moon, V., Bradshaw, J., Smith, R., & de Lange, W. (2005). Geotechnical characterisation of stratocone crater wall sequences, White Island Volcano, New Zealand. *Engineering Geology*, *81*(2), 146–178.

Mordret, A., Jolly, A. D., Duputel, Z., & Fournier, N. (2010). Monitoring of phreatic eruptions using interferometry on retrieved cross-correlation function from ambient seismic noise: Results from Mt. Ruapehu, New Zealand. *Journal of Volcanology and Geothermal Research*, *191*(1-2), 46–59. https://doi.org/10.1016/j.jvolgeores.2010.01.010

Nishi, Y., Sherburn, S., Scott, B. J., & Sugihara, M. (1996). High-frequency earthquakes at White Island volcano, New Zealand: Insights into the shallow structure of a volcano-hydrothermal system. *Journal of Volcanology and Geothermal Research*, *72*(3-4), 183–97.

Niu, F., Silver, P. G., Daley, T. M., Cheng, X., & Majer, E. L. (2008). Preseismic velocity changes observed from active source monitoring at the Parkfield SAFOD drill site. *Nature*, *454*(7201), 204–208.

Nur, A. (1971). Effects of stress on velocity anisotropy in rocks with cracks. *Journal of Geophysical Research*, *76*(8), 2022–2034. https://doi.org/10.1029/JB076i008p02022

Nur, A., & Simmons, G. (1969a). Stress-induced velocity anisotropy in rock: An experimental study. *Journal of Geophysical Research*, *74*(27), 6667.

Nur, A., & Simmons, G. (1969b). The effect of saturation on velocity in low porosity rocks. *Earth and Planetary Science Letters*, *7*, 183–193.

Obermann, A., Planès, T., Larose, E., & Campillo, M. (2013). Imaging preeruptive and coeruptive structural and mechanical changes of a volcano with ambient seismic noise. *Journal of Geophysical Research: Solid Earth*, *118*, 6285–6294. https://doi.org/10.1002/2013JB010399

Patanè, D., De Gori, Pasquale, Chiarabba, C., & Bonaccorso, A. (2003). Magma ascent and the pressurization of Mount Etna's volcanic system. *Science*, *299*(5615), 2061–2063.

Poupinet, G., Ellsworth, W. L., & Frechet, J. (1984). Monitoring velocity variations in the crust using earthquake doublets: An application to the Calaveras Fault, California. *Journal of Geophysical Research*, *89*(B7), 5719–5731. https://doi.org/10.1029/JB089iB07p05719

Ratdomopurbo, A., & Poupinet, G. (1995). Monitoring a temporal change of seismic velocity in a volcano: Application to the 1992 eruption of Mt. Merapi (Indonesia). *Geophysical Research Letters*, *22*(7), 775–778.

Richter, T., Sens-schönfelder, C., Kind, R., & Asch, G. (2014). Comprehensive observation and modeling of earthquake and temperature-related seismic velocity changes in northern Chile with passive image interferometry. *Journal of Geophysical Research: Solid Earth*, *119*, 4747–4765. https://doi.org/10.1002/2013JB010695

Rivet, D., Brenguier, F., & Cappa, F. (2015). Improved detection of preeruptive seismic velocity drops at the Piton de La Fournaise volcano. *Geophysical Research Letters*, *42*, 6332–6339. https://doi.org/10.1002/2015GL064835

Sabra, K. G., Gerstoft, P., Roux, P., Kuperman, W. A., & Fehler, M. C. (2005). Extracting time-domain Green's function estimates from ambient seismic noise. *Geophysical Research Letters*, *32*, L03310. https://doi.org/10.1029/2004GL021862

Schimmel, M., & Paulssen, H. (1997). Noise reduction and detection of weak, coherent signals through phase weighted stacks. *Geophysical Journal International*, *130*, 497–505.

Sens-Schönfelder, C., & Wegler, U. (2006). Passive image interferemetry and seasonal variations of seismic velocities at Merapi Volcano, Indonesia. *Geophysical Research Letters*, *33*, L21302. https://doi.org/10.1029/2006GL027797

Shapiro, N. M., & Campillo, M. (2004). Emergence of broadband Rayleigh waves from correlations of the ambient seismic noise. *Geophysical Research Letters*, *31*, L07614. https://doi.org/10.1029/2004GL019491

Shapiro, N. M., Campillo, M., Stehly, L., & Ritzwoller, M. H. (2005). High-resolution surface-wave tomography from ambient seismic noise. *Science*, *307*(5715), 1615–1618.

Sherburn, S., Scott, B. J., Nishi, Y., & Sugihara, M. (1998). Seismicity at White Island volcano, New Zealand: A revised classification and inferences about source mechanism. *Journal of Volcanology and Geothermal Research*, *83*(3-4), 287–312.

Silver, P. G., Daley, T. M., Niu, F., & Majer, E. L. (2007). Active source monitoring of cross-well seismic travel time for stress-induced changes. *Bulletin of the Seismological Society of America*, *97*(1B), 281–293.

Snieder, R. (2006). The theory of coda wave interferometry. *Pure and Applied Geophysics*, *163*(2-3), 455–473.

Sparks, R. S. J. (2003). Forecasting volcanic eruptions. *Earth and Planetary Science Letters*, *210*(1-2), 1–15.

Takano, T., Nishimura, T., Nakahara, H., Ohta, Y., & Tanaka, S. (2014). Seismic velocity changes caused by the Earth tide: Ambient noise correlation analyses of a small array data. *Geophysical Research Letters*, *41*, 6131–6136. https://doi.org/10.1002/2014GL060690

Wang, Q. Y., Brenguier, F., Campillo, M., Lecointre, A., Takeda, T., & Aoki, Y. (2017). Seasonal crustal seismic velocity changes throughout Japan. *Journal of Geophysical Research: Solid Earth*, *122*, 7987–8002. https://doi.org/10.1002/2017JB014307

Yamamura, K., Sano, O., Utada, H., Takei, Y., Nakao, S., & Fukao, Y. (2003). Long-term observation of in situ seismic velocity and attenuation. *Journal of Geophysical Research*, *108*(B6), 2317. https://doi.org/10.1029/2002JB002005

Yates, A. S. (2018). Seismic velocity changes at White Island volcano from ambient noise interferometry (Master's thesis). NZ: Victoria University of Wellington.